

# Statistical-based Deformable Models with Simultaneous Optimization of Object Gray-level and Shape Characteristics

S. S. Gleason  
Oak Ridge National Laboratory  
P.O. Box 2008  
Oak Ridge, TN 37831-6011  
gleasonss@ornl.gov

H. Sari-Sarraf  
Texas Tech University  
Electrical Engineering Department  
Lubbock, Texas, 79409-3102  
hamed.sari-sarraf@coe.ttu.edu

M. A. Abidi  
The University of Tennessee  
Electrical Engineering Department  
Knoxville, Tennessee, 37996-2100  
mabidi@utk.edu

M. J. Paulus (paulusmj@ornl.gov) D. K. Johnson (johnsondk@ornl.gov)  
Oak Ridge National Laboratory

## Abstract

*A statistical-based deformable model is being developed that improves upon existing point distribution models (PDMs). Existing PDM boundary finding techniques often suffer from the following shortcomings: (1) a priori local shape characteristics are not utilized, (2) global shape and gray-level information are treated independently during boundary optimization, and (3) there is no existing metric that provides a confidence measure of segmentation performance. A new deformable model algorithm is under development in which the objective function used during optimization of the boundary encompasses several important characteristics. First the objective function includes both global shape and local gray-level characteristics, so optimization occurs with respect to both pieces of information simultaneously. In addition, local shape characteristics, as derived from the training set, are also incorporated into the boundary finding process. Finally, the objective function is formulated in a way that leads to a confidence metric that indicates how well the final boundary fits the underlying object as defined in the target image. This new algorithm is being applied to geometric test images as well as high-resolution x-ray computed tomography (CT) images of laboratory mice for the purpose of organ identification.*

## 1. Introduction

A new statistical-based deformable model algorithm for image analysis is being developed. The motivation for this work is the need for an algorithm to perform automatic segmentation and recognition of semi-rigid objects with faint, missing, or obstructed edges within a complex background. Semi-rigid objects are those that demonstrate controlled shape variability over multiple instances of that object. An example of this type of application presented in this paper is the segmentation/recognition of organs (skull, heart, lung, and kidneys) within medical imagery (x-ray CT cross-sections of mice). After substantial investigation of a variety of segmentation algorithms, a statistical-based deformable

model, the active shape model (ASM) developed by Cootes, et al. [1], was chosen as an appropriate starting point because of its ability to incorporate *a priori* information extracted from a training set to build a gray-level model (GLM) and a shape model (SM). These models are used during an iterative contour deformation process that adjusts the position and shape of the contour to match the boundary of the object within the image. Although ASM is an excellent starting point for the motivating application, it has shortcomings in a few key areas: (1) *a priori* local shape characteristics are not utilized, (2) global shape and gray-level information are treated independently during optimization of the boundary position, and (3) there is no existing metric that provides a confidence measure of segmentation performance. These shortcomings limit ASM's robustness and accuracy in some applications, such as the medical image analysis application introduced later in this paper. The new algorithm being developed will address each these shortcomings, and, hence, will be a more effective statistical-based deformable model algorithm.

A few researchers have recently developed new statistical-based deformable models based on ASM. Wang, et al. [2] have developed a probabilistic based optimization scheme that uses Cootes' PDM and integrates Canny-edge information into the maximum *a posteriori* (MAP) objective function as the underlying image attraction force. Kervrann, et al. [3] have developed similar probabilistic techniques, but include Markov modeling on the local scale to promote boundary smoothness. Both of these ASM adaptations rely on edge information in the target image as the external attraction force, rather than the gray-level gradients proposed by Cootes. Duta, et al. [4] have also refined the ASM technique in terms of the image attraction force as well as the optimization approach to fit the boundary to the underlying image data. Consideration of boundary-point outliers is an important consideration in their work. Even with the considerable research that has been performed, none of the resulting approaches address the three shortcomings of existing PDMs outlined previously.

## 2. Improved Statistical Shape Model

The following formulation is similar to that presented in [1]. Let the manually selected boundary, or shape, for the  $i^{\text{th}}$  image in an  $M$ -image training set be represented by a collection of aligned landmark points (LPs),  $L(i)$  as in eqn. (1).

$$L(i) = [x_1(i), x_2(i), \dots, x_N(i), y_1(i), y_2(i), \dots, y_N(i)]'; \quad (1)$$

$$\forall i = 1, \dots, M$$

where the  $N$  LPs are defined by the coordinate pairs

$$\{x_j(i), y_j(i)\}; \forall j = 1, \dots, N. \quad (2)$$

Once selected by the user, the alignment of the  $L(i)$ s to a common coordinate frame is done via Procrustes analysis [7]. Note that a boundary,  $L(i)$ , may be composed of any number of open and/or closed boundaries. This is an often overlooked, but extremely useful characteristic of this boundary modeling technique that allows great flexibility for the user during training, yet does not complicate the boundary optimization process.

Using this training data set of aligned  $L(i)$ s, we can create a global shape model (GSM) by using principal component analysis (PCA) to formulate an expression that represents a new shape,  $L$ , as

$$L = \bar{L} + \Phi b = \bar{L} + \begin{bmatrix} \phi_1 & \dots & \phi_{t_s} \end{bmatrix} \begin{bmatrix} b_1 \\ \dots \\ b_{t_s} \end{bmatrix}, \quad (3)$$

where  $\bar{L}$  is the mean of the  $L(i)$ ,  $\Phi$  is a matrix whose columns are the eigenvectors ( $\phi_k$  for all  $k=1\dots t_s$ ) corresponding to the  $t_s$  largest eigenvalues ( $\lambda_k$ , for all  $k=1\dots t_s$ ) of the covariance matrix for the collection of  $L(i)$ ,  $i=1\dots M$ . The value of  $t_s$  is typically chosen to capture  $\sim 98\%$  of the total variation in the training set. The elements of  $b$  govern the amount of shape variation from the mean,  $\bar{L}$ , along each eigenvector. Alternatively, given a shape,  $L$ , one can transform that shape into the PCA sub-space using the equation

$$b = \Phi'(L - \bar{L}). \quad (4)$$

Also, as part of the training process, gray-level profiles,  $g(i)(j)$ , ( $i=1\dots M$ ,  $j=1\dots N$ ) are extracted from each of the  $M$  training images along lines through each of the  $N$  LPs, normal to the boundary. These profiles can be expressed as

$$g(i)(j)_k = I_i \left( x_j(i) - \left( \frac{N_g - 1}{2} - k + 1 \right) \cos \alpha_j(i), \right. \quad (5)$$

$$\left. y_j(i) - \left( \frac{N_g - 1}{2} - k + 1 \right) \sin \alpha_j(i) \right); \forall k = 1, \dots, N_g$$

where  $I_i$  is the  $i^{\text{th}}$  image in the training set,  $N_g$  is the number of gray-level samples in each profile, and  $\alpha_j(i)$  is the angle of the profile through the  $j^{\text{th}}$  LP normal to the boundary. A improvement in numerical stability was made to the published ASM gray-level modeling approach [1] in that a new gray-level model (GLM) is formulated by performing PCA on each set of gray-level training profiles for a given LP. Similar to eqn. (3), we can represent a new gray-level profile,  $g(j)$ , through the  $j^{\text{th}}$  LP as

$$g(j) = \overline{g(j)} + \Psi(j)d(j) \quad (6)$$

$$= \overline{g(j)} + \begin{bmatrix} \Psi(j)_1 & \dots & \Psi(j)_{t_g(j)} \end{bmatrix} \begin{bmatrix} d(j)_1 \\ \dots \\ d(j)_{t_g(j)} \end{bmatrix}$$

where  $\overline{g(j)}$  is the mean of the  $M$  training profiles through the  $j^{\text{th}}$  LP,  $\Psi(j)$  is a matrix whose columns are the eigenvectors ( $\Psi(j)_k$  for all  $k=1\dots t_g(j)$ ) corresponding to the  $t_g(j)$  largest eigenvalues ( $\lambda_{g_k}$  for all  $k=1\dots t_g(j)$ ) of the covariance matrix for the collection of  $g(i)(j)$ ,  $i=1\dots M$ . This covariance matrix, which was used directly in the original ASM formulation [1], was nearly singular for several image training sets used during the initial testing. This singularity prompted the development of the PCA approach for the GLM. The elements of  $d(j)$  govern the amount of variation from the mean gray-level profile,  $\overline{g(j)}$ , along each eigenvector. Similar to the GSM, given a gray-level profile,  $g(j)$ , one can transform that profile into the PCA sub-space using the equation

$$d(j) = \Psi'(j)(g(j) - \overline{g(j)}). \quad (7)$$

Some additional improvements were made to the ASM approach including:

1. incorporation of resolution dependence into the GSM and
2. an improved GLM that includes both gradient and absolute intensity terms.

For more technical detail about these improvements see [5]. Using the described GSM and GLM formulations and the optimization approach outlined in [1], several segmentation experiments were carried out. Two successful segmentation results on x-ray CT cross sections of laboratory mice are shown in Fig. 1 and Fig. 2. The images were acquired using a micro CT system developed at Oak Ridge National Laboratory [6].

Although good results were achieved on some of the test cases, this improved statistical shape model still suffers from the key shortcomings previously mentioned: there is no con-

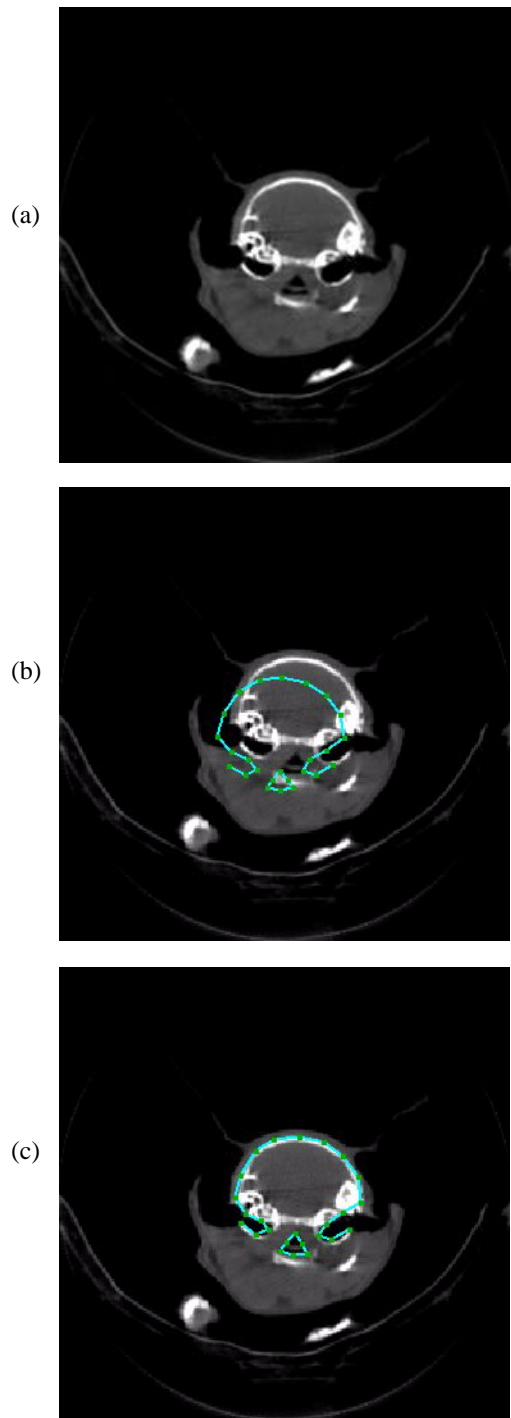


Figure 1. Skull-ear canal segmentation result using improved ASM algorithm. (a) shows the original image, (b) shows the initial shape model position, and (c) shows the final result after fitting the model to the image data.

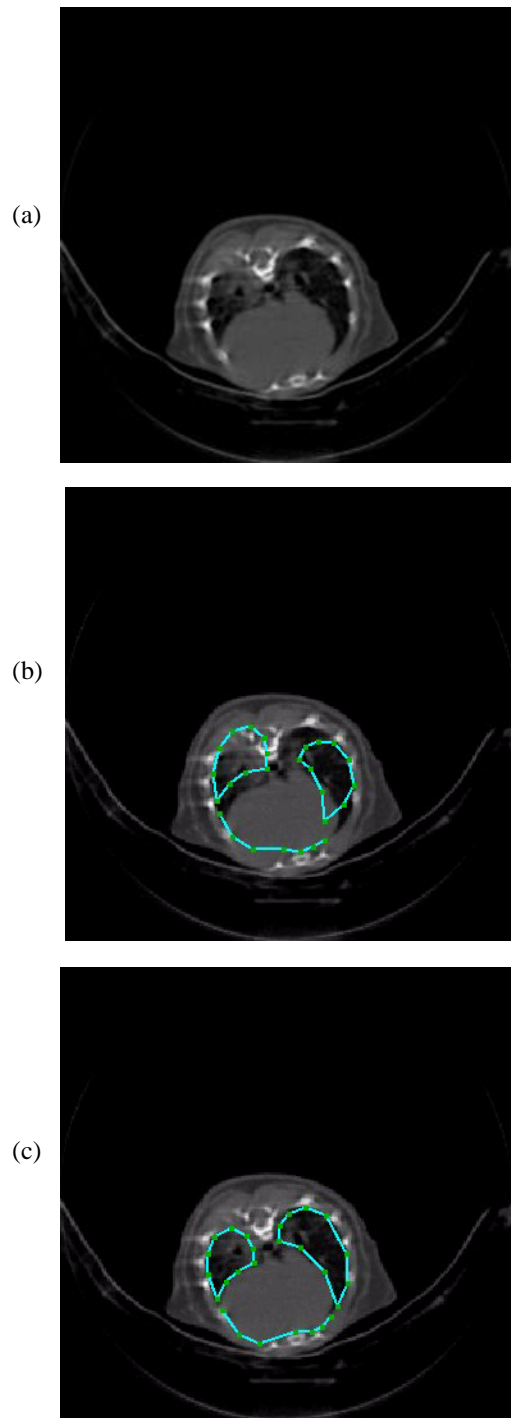


Figure 2. Heart-lung segmentation result using improved ASM algorithm. (a) shows the original image, (b) shows the initial shape model position, and (c) shows the final result after fitting the model to the image data.

sideration of local shape features, the GSM and GLM are optimized independently, and there is no confidence metric generated that estimates the goodness of boundary fit to the image data.

### 3. Local Shape Modeling

In published descriptions of the ASM training procedure, authors commonly describe the LP labelling process in two steps. First, “critical” LPs are placed on key features of the object such as corners, high curvature features, etc. Second, additional “interpolation” LPs are distributed along the boundary between the critical LPs. Although this distinction is made between the two type of LPs during manual boundary placement, both sets of LPs are treated identically throughout the remainder of the training and optimization processes. Hence, the important local shape information the user is attempting to preserve around the critical LPs is deemphasized when all LPs (both critical and interpolated) are lumped into a single global model of shape, the GSM.

We propose the introduction of local shape models (LSMs) that preserve the local shape information around each user-defined critical LP. This formulation is similar to the GSM formulation in that a subset of local-shape LPs,  $l(i)(j)$ , is identified in the neighborhood of each critical LP during training, where

$$l(i)(j) \subset L(i); \forall i = 1, \dots, M; \forall j = 1, \dots, N_c, \quad (8)$$

and  $N_c$  is the number of user-defined critical LPs. Before generating the LSM, these subsets of points must be aligned to a common coordinate frame. We will call the aligned set of LPs  $\hat{l}(i)(j)$  where

$$\hat{l}(i)(j) = [\hat{x}_{h(j)}(i), \dots, \hat{x}_{h(j)+N_l-1}(i), \hat{y}_{h(j)}(i), \dots, \hat{y}_{h(j)+N_l-1}(i)] \quad (9)$$

$h(j)$  defines the index of the first local-shape LP in the boundary,  $L(i)$ , belonging to the  $j^{\text{th}}$  local shape, and  $N_l$  is the number of LPs in each local shape. Similar to the GSM and GLM, we can represent a new set of local-shape LPs,  $\hat{l}(j)$ , using the expression

$$\begin{aligned} \hat{l}(j) &= \overline{\hat{l}(j)} + \Omega(j)c(j) \\ &= \overline{\hat{l}(j)} + \begin{bmatrix} \omega(j)_1 & \dots & \omega(j)_{t_l(j)} \end{bmatrix} \begin{bmatrix} c(j)_1 \\ \dots \\ c(j)_{t_l(j)} \end{bmatrix} \end{aligned} \quad (10)$$

where  $\overline{\hat{l}(j)}$  is the mean of all the aligned local-shape LP subsets,  $\hat{l}(i)(j)$ , for the  $j^{\text{th}}$  critical LP. The columns of the matrix  $\Omega(j)$  are the eigenvectors ( $\omega(j)_k$  for all  $k=1\dots t_l(j)$ ) corresponding to the  $t_l(j)$  largest eigenvalues ( $\lambda_{t_k}$  for all  $k=1\dots t_l(j)$ ) of the covariance matrix for the collection of  $\hat{l}(i)(j)$ ,  $j=1,\dots,M$ . The elements of  $\overline{c(j)}$  govern the amount of shape variation from the mean,  $\overline{\hat{l}(j)}$ , along each eigenvector. Once again, similar to the GSM and GLM, given a set of local-shape LPs,  $\hat{l}(j)$ , one can transform that shape into the PCA sub-space using the equation

$$c(j) = \Omega(j)'(\hat{l}(j) - \overline{\hat{l}(j)}). \quad (11)$$

The incorporation of these LSMs into a new optimization scheme that fits a boundary to the image data is described next.

### 4. Objective Function Formulation

As mentioned previously, the original ASM boundary fitting scheme optimizes the GSM and GLM independently. This leads to problems in that the optimal boundary selection will be biased towards either the GSM or the GLM instead of considering both equally. Consider the plot of a GLM objective function in Fig. 3. Note that there are two local minima

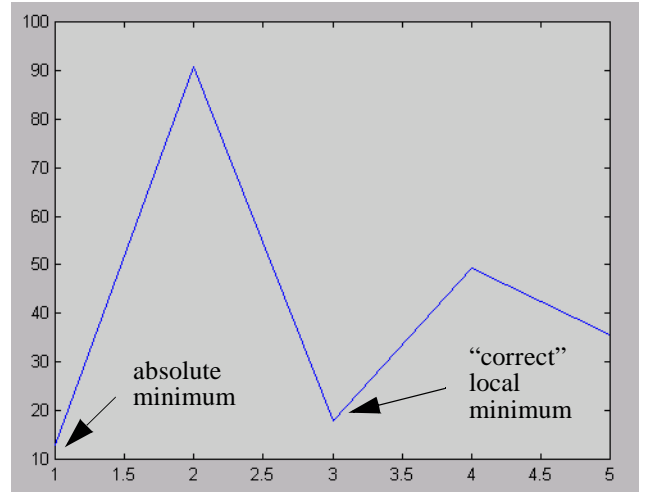
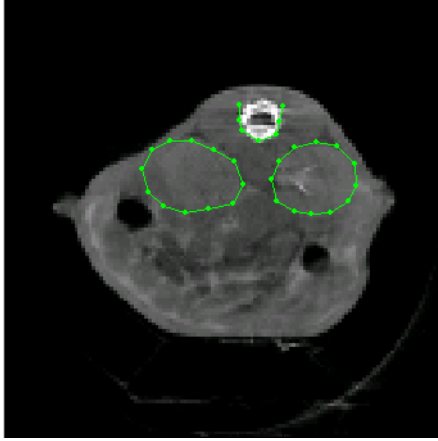


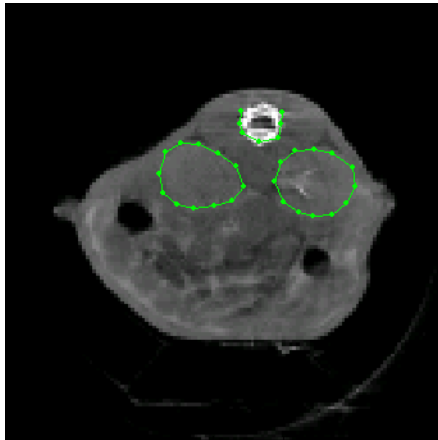
Figure 3. Plot of the value of the GLM objective function (y-axis) versus relative pixel position of an LP (x-axis) for a given test image.

that result in similar values of the objective function, so that both indicate LP positions that are a good fit to the GLM. One of the local minima will generate a boundary that fits the GSM very well (the one on the right), while the other local minimum (the absolute minimum) creates a boundary that does not fit the GSM. Because the GLM objective function is considered independently from the GSM, the absolute minimum is selected, leading to the segmentation result in

Fig. 4(a). If, on the other hand, the local minimum is manually selected to best satisfy both the GLM and GSM, the segmentation result in Fig. 4(b) is achieved. In addition, recall that a third component, the LSM, needs to be added to the optimization scheme. A single objective function is needed that encompasses the *a priori* information captured by the GSM, GLM, and LSM, and allows the generation of a confidence metric. This objective function is developed next.



(a)



(b)

Figure 4. Kidney and spine segmentation via (a) independent optimization of the GLM and SM and (b) simultaneous optimization of both the GLM and SM. Note the incorrect segmentation of the left kidney in (a).

Similar to that presented in [2], a shape parameter vector,  $v$ , is formed that combines both PCA shape information as well as boundary pose data as

$$v = \begin{bmatrix} b' \\ p' \end{bmatrix}, \quad (12)$$

where

$$p = \begin{bmatrix} s \\ \theta \\ T_x \\ T_y \end{bmatrix}', \quad (13)$$

$s$  is scale,  $\theta$  is rotation, and  $T_x, T_y$  are the  $x$ - and  $y$ -translations of the boundary. Now, using Bayes rule, we can write the maximum *a posteriori* (MAP) probability of a shape parameter vector,  $v$ , given an image,  $I$ , as

$$Pr(v|I) = \frac{Pr(I|v)Pr(v)}{Pr(I)}. \quad (14)$$

We can express the prior shape probability,  $Pr(v)$ , as an independent combination of the global and local shape probabilities

$$Pr(v) = Pr_g(v)Pr_l(v). \quad (15)$$

Assuming a multivariate Gaussian distribution for the GSM parameters,  $v_i, i=1\dots t_s$ , we can write

$$Pr_g(v) = \prod_{i=1}^{t_s} \frac{1}{\sqrt{2\pi}\sigma(v_i)} \exp\left\{-\frac{(v_i - \bar{v}_i)^2}{2\sigma(v_i)^2}\right\}. \quad (16)$$

Similarly, assuming independence of LSMs and a Gaussian distribution for each LSM, we can write

$$Pr_l(v) = \prod_{i=1}^{N_c} \prod_{j=1}^{t_l(i)} \frac{1}{\sqrt{2\pi}\sigma(c(i)_j)} \exp\left\{-\frac{(c(v, i)_j - \overline{c(i)_j})^2}{2\sigma(c(i)_j)^2}\right\} \quad (17)$$

where  $c(i)$  has been re-written as  $c(v, i)$  to indicate that it is a function of the shape parameter vector (boundary),  $v$ .

We now have completely specified our shape prior (global and local),  $Pr(v)$ , so we turn our attention to the likelihood term,  $Pr(I|v)$ . This term expresses the probability of extracting a set of gray-level profiles from the image,  $I$ , given a shape parameter vector,  $v$ . Assuming independence of the profile-based GLMs for each LP, we can write

$$Pr(I|v) = \prod_{i=1}^N Pr(g(v, i)). \quad (18)$$

where  $g(i)$  has been re-written as  $g(v, i)$  to indicate that it is a function of the shape parameter vector,  $v$ . Once again we assume (as in [1]) that the gray-level profiles for the  $i^{\text{th}}$  LP

can be modeled by a multivariate Gaussian distribution, and write

$$Pr(g(v, i)) = \frac{1}{(2\pi)^{N_g/2} |G(i)|^{1/2}} \times \exp\left\{-\frac{(g(v, i) - \overline{g(i)})' K(i) (g(v, i) - \overline{g(i)})}{2}\right\} \quad (19)$$

where

$$K(i) = \frac{1}{\sigma_g(i)} (I - \Psi(i)\Psi'(i)) + \Psi(i)\Lambda(i)\Psi'(i), \quad (20)$$

$\sigma_g(i)$  is the variance of the residual, and the diagonal matrix,  $\Lambda(i)$ , has diagonal elements

$$diag \Lambda(i) = \left[ \frac{1}{\lambda_g(i)_1} \frac{1}{\lambda_g(i)_2} \dots \frac{1}{\lambda_g(i)_{t_g(i)}} 0 \dots 0 \right]. \quad (21)$$

We now have expressions for all probability terms in our Bayesian formulation given by eqn. (14). To form the objective function,  $J(v)$ , we take the log as follows

$$J(v) = \ln Pr(v|I) = \ln Pr_g(v) + \ln Pr_I(v) + \ln Pr(I|x). \quad (22)$$

By simplifying and removing all terms that are independent of  $v$ , we are left with three terms:  $J_1$ ,  $J_2$ , and  $J_3$  that satisfy

$$J(v) = J_1(v) + J_2(v) + J_3(v) \quad (23)$$

where

$$J_1(v) = -\sum_{i=1}^t \frac{(v_i - \overline{v}_i)^2}{2\sigma(v_i)^2}, \quad (24)$$

$$J_2(v) = -\sum_{i=1}^{N_c} \sum_{j=1}^{t(i)} \frac{(c(v, i)_j - \overline{c(i)_j})^2}{2\sigma(c(i)_j)^2}, \text{ and} \quad (25)$$

$$J_3(v) = -\frac{1}{2} \sum_{i=1}^N (g(v, i) - \overline{g(i)})' K(i) (g(v, i) - \overline{g(i)}). \quad (26)$$

As designed,  $J$  has one term for each of the trained models: GSM ( $J_1$ ), LSM ( $J_2$ ), and GLM ( $J_3$ ).

## 5. Preliminary Results

The gradient of  $J$  was calculated analytically and a gradient descent program was written to minimize  $J$  with respect to the shape parameter vector,  $v$ . At this point some

very simple geometric shapes have been tested to help debug the implementation, validate the approach, and investigate the behavior of  $J$ . These results are shown in Fig. 5.

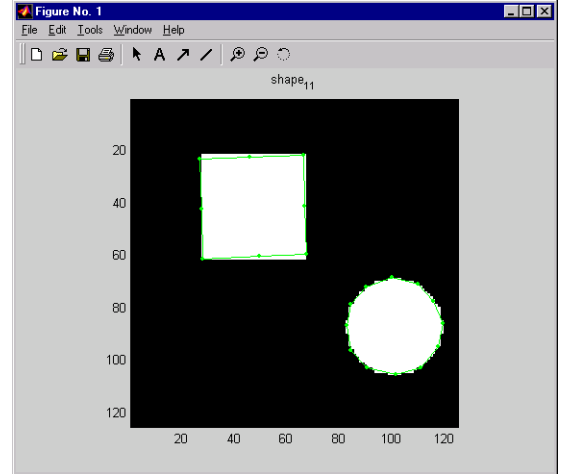
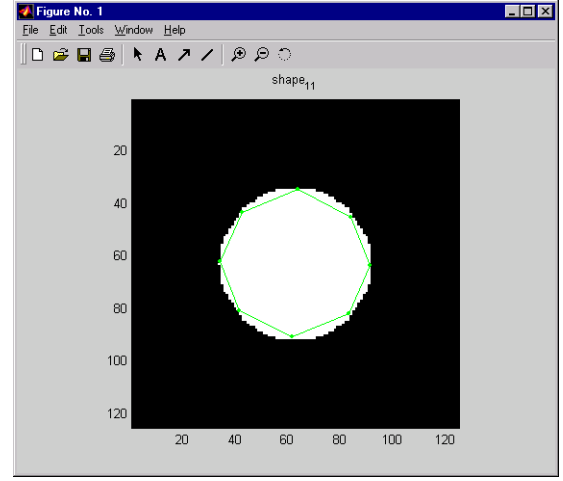


Figure 5. Preliminary segmentation results using the new shape model optimization approach.

## 6. Conclusions and Future Work

A theoretical formulation for a new statistical shape model has been presented that has several improvements over similar techniques. Most notable are (1) the incorporation of a mechanism to model local shape characteristics, (2) the formulation of an objective function that allows simultaneous optimization of the GSM, LSM, GLM, and (3) the probabilistic nature of the objective function which lends itself well to the generation of a segmentation confidence metric.

Clearly there is work to be done to validate this new objective function on more complex image data. Furthermore, a clearer understanding of the behavior of the objective function,  $J$ , (e.g. presence of local minima) is needed to predict the applicability of this approach to a variety of image types. Also, the exact formulation of the segmentation confidence metric must be determined. Finally, a direct comparison of the presented approach to existing techniques in terms of segmentation accuracy, speed, robustness, etc., is needed.

## 7. References

- [1]. T. Cootes, C. Taylor, D. Cooper, and J. Graham, "Active shape models — their training and application", *Computer Vision and Image Understanding*, vol. 61, n. 1, pp. 38-59, Jan. 1995.
- [2]. Y. Wang and L. Staib, "Boundary finding with correspondence using statistical shape models", *IEEE Proc. Computer Vision and Pattern Recognition*, pp. 338-345, 1998.
- [3]. C. Kervrann and F. Heitz, "A hierarchical markov modeling approach for the segmentation and tracking of deformable shapes", *Graphical Models and Image Processing*, vol. 60, n. 3, pp. 173-195, May 1998.
- [4]. N. Duta and M. Sonka, "Segmentation and interpretation of MR brain images: an improved active shape model", *IEEE Trans. on Medical Imaging*, vol. 17, no. 6, December 1998.
- [5]. S. Gleason, H. Sari-Sarraf, M. Paulus, D. Johnson, M. Abidi, "Automatic screening of polycystic kidney disease in x-ray CT images of laboratory mice," *Proc. SPIE Medical Imaging Conf.*, February, 2000.
- [6]. M. Paulus, H. Sari-Sarraf, S. Gleason, M. Bobrek, J. Hicks, D. Johnson, J. Behel, and L. Thompson, "A new x-ray computed tomography system for laboratory mouse imaging," *IEEE Trans. on Nucl. Science*, July, 1999.
- [7]. C. Goodall, "Procrustes Methods in the Statistical Analysis of Shape," *Journal of the Royal Statistical Society B*, 53(2):285-339, 1991.